A comparative study of modelling RC slab response to blast loading with two typical concrete material models

A comparative study of modelling RC slab response to blast loading with two typical concrete material models

Jiaming Xu, Yong Lu*

Institute for Infrastructure and Environment, School of Engineering, The University of Edinburgh, The Kings Buildings, Edinburgh EH9 3JL, UK

* Correspondence: yong.lu@ed.ac.uk

Abstract

The soundness of numerical simulation for reinforced concrete structures under blast loading is closely related to the capacity of the concrete models in dealing with the nonlinear behaviour of the material under complex stress conditions. To understand more comprehensively the demands a rigorous simulation may impose on a modelling approach and thereby the needs for improvement in the model formulation, a comparative numerical simulation study has been conducted in which two representative concrete material models, namely KCC and CSC models, are employed to model a typical RC slab subjected to blast load. For such a classical modelling situation, the model with KCC concrete material tends to fail prematurely with a total global failure of the slab, which is not consistent either with the experimental observations or with the CSC modelling results. Extensive analysis of the failure processes reveals that the abnormal response in the KCC model is linked to the rapid descending of the material model behaviour towards an effectively zero stress state following a tension/shear controlled damage process, and the consequent diminish of the interaction capacity between the steel rebar and the surrounding concrete. The findings from this study points a direction in which certain rectification will need to be considered in order to ensure a reliable modelling outcome with the KCC type concrete models in simulating the response RC structures, both globally and locally.

1. Introduction

Concrete is commonly used in civil and defence constructions. The behaviour of concrete material and reinforced concrete structures under impact and blast loads has attracted much renewed research interest in recent years. A distinctive trend in the latest research effort on this subject is an ever increased use of high fidelity numerical simulation approaches. Apart from the traditional rationale in connection with all the difficulties and costs involved in

conducting full or reduced-scale field tests, the temptation towards computer simulation has been promoted by the availability of advanced dynamic analysis codes and the growing computer power, which have made it possible to carry out rather sophisticated numerical analyse with a desk-top computer.

It is generally understood, on the other hand, that the response of concrete structures to impact and blast loads is complicated and it involves a number of challenges in terms of the rigour and reliability of modelling considerations, for example appropriate handling of pressure and rate dependence of materials, stress wave phenomenon, damage evolution and softening, as well as large deformations. Although these capabilities have mostly been incorporated in various general-purpose computational analysis software (e.g. LS-DYNA [1], Autodyn [2], ABAQUS/Explicit [3]), whether or not the underlying mechanics during the dynamic process may be adequately represented still depends on the soundness of the constitutive material descriptions and the interactions among the constituent materials under the complex structural and loading environment, as well as the ability of the analyst in comprehending the model behaviour and interpreting the analysis results.

Different computational techniques exist for the analysis of concrete structures under high dynamic loading [4]. Nonetheless, the majority of the numerical simulation studies in this field are conducted using a finite element approach. In a traditional continuum FE framework, fracture of concrete is simulated in a smeared manner using the so-called macro-scale material models, in which classical continuum mechanics based considerations, e.g. damage evolution, plastic flow, failure surfaces and so on are implemented at the local element level. Mesh-objective softening (i.e. preservation of the fracture energy) may be achieved by incorporating a mesh-adjusted softening rule (e.g. KCC [5], CSC [6]).

Numerous studies, including some of the work done by this group, have been carried out recently to examine and verify numerical models developed under such a general FE framework for high impulsive loading analysis (e.g. [4,7,8]). It has been found that the outcome of a numerical simulation is closely related to the capacity of the concrete models in dealing with the nonlinear behaviour of the material under complex loading conditions, and in the analyses involving the direct effects of a blast or impact load some typical concrete models, for example the Concrete Damage model in LS-DYNA and the RHT model in Autodyn, are found to generally perform satisfactorily [4,9]. However, it should be borne in mind that the performance of a particular material model could vary in different

structural and loading conditions. Therefore continued research effort is needed to understand more comprehensively the demands a rigorous simulation may impose on a modelling approach and thereby the needs for improvement in the model formulation.

This paper is mainly concerned about the performance of concrete material models when applied in the simulation of reinforced concrete (RC) structures under blast loading. Two representative concrete models, namely Concrete Damage Model (also known as KCC model) [5] and Continuous Surface Concrete Model [6] (known as CSC model), both available in LS-DYNA [1], are employed and examined. The detailed simulations are carried out using respectively the two material models on a RC slab that was physically tested under blast load.

The overall structural response in such a loading scenario is understood to be primarily monotonic, and consequently the performance of these material models are expected not to differ significantly from what have been observed in other reported simulation studies. However, it has been discovered, rather surprisingly, that the KCC model could not produce a sensible result especially in the later stage of the response, whereas the CSC model exhibits reasonable performance throughout the entire response.

Securitisation of the detailed response in relation to the basic behaviour of the material model behaviour suggests that the root cause of the problem tends to originate from the faster descending of the material model behaviour towards an effectively zero strength state following a tension/shear dominated damage process, and the consequent diminish of the interaction capacity between the steel rebar and the surrounding concrete. In contract, the CSC model retains a certain level of residual capacity which enables a minimum connection between the rebar and the surrounding concrete at the severely cracked but not entirely fragmented state. In a broader sense, necessary rectification would need to be considered when it comes to using the KCC type model in simulating the response of RC structure concerning both global and local responses.

2. Modelling of RC slab response to blast load

2.1 Experimental background

The simulation is conducted on a prototype RC slab, which was tested at the University of Missouri Kansas City (UMKC) as described in [10]. The tests were conducted using a Blast Loading Simulator (BLS), which is capable of simulating a uniform pressure pulse on the

loading face. The test slab was supported against two strong steel box beams on the rear side of the slab, and the response of the slab was measured by accelerometers and laser measurement device attached to the rear face of the slab. High speed cameras were also used to record the response of the slab.

Fig. 1 shows the geometry and reinforcement details of the RC slab simulated in this study. Based on the experiment [10], the material properties assumed here include normal concrete of 30MPa, and reinforcing steel rebar of grade 410MPa in both transverse and longitudinal directions. The reinforcement is placed only on the bottom (opposite to loading) side of the slab. The general observation from the experiment indicated extensive cracking at the peak deformation but no total global failure occurred. It should be noted that the present study focuses on the comparative response in the numerical simulations using respectively two concrete material models, therefore it was not intended (nor deemed necessary) to pursue a detailed comparison with the background experiment.

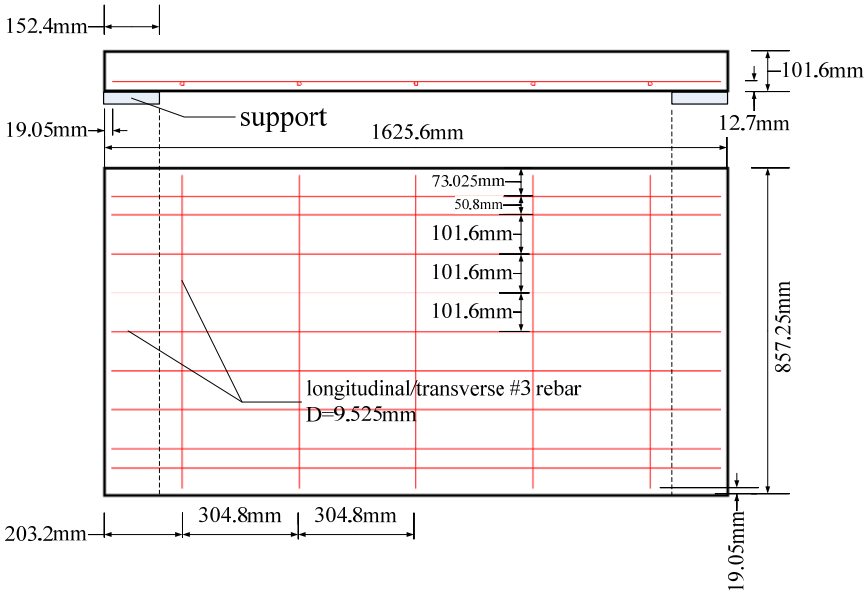

Figure 1. Geometry and reinforcement details of the RC slab (adapted from [10])

2.2 General model settings

The numerical simulation is carried out using LS-DYNA [1]. In the finite element model for the RC slab, 8-node solid elements are used for concrete whilst 2-node beam elements are used for longitudinal and transverse reinforcements. The beam elements for the rebar are embedded in the solid elements and therefore nodes are shared between the rebar and

concrete elements along the length of the rebar. This treatment is equivalent to assuming a perfect bond between rebar and the surrounding concrete, which is commonly adopted in the modelling of RC structural response to blast type of loads. The basic rationale is that the response during the loading phase is so fast that there is no time for “slip” to develop, whereas in the subsequent phase bond failure and “slip” may be reasonably represented through the softening and failure of the concrete to which the rebar is attached. Considering symmetry, only a quarter of the slab needs to be modelled. The layout of the ¼ RC slab model including the end support steel beam is illustrated in Fig. 2.

Trial analyses were conducted to examine the sensitivity of the computed results to the mesh size and an average element length of 6.35mm (1/4 in) was chosen. This offers a resolution of 16 solid elements along the slab thickness, with a total of 812 beam elements for rebars and about 150,000 solid elements for concrete.

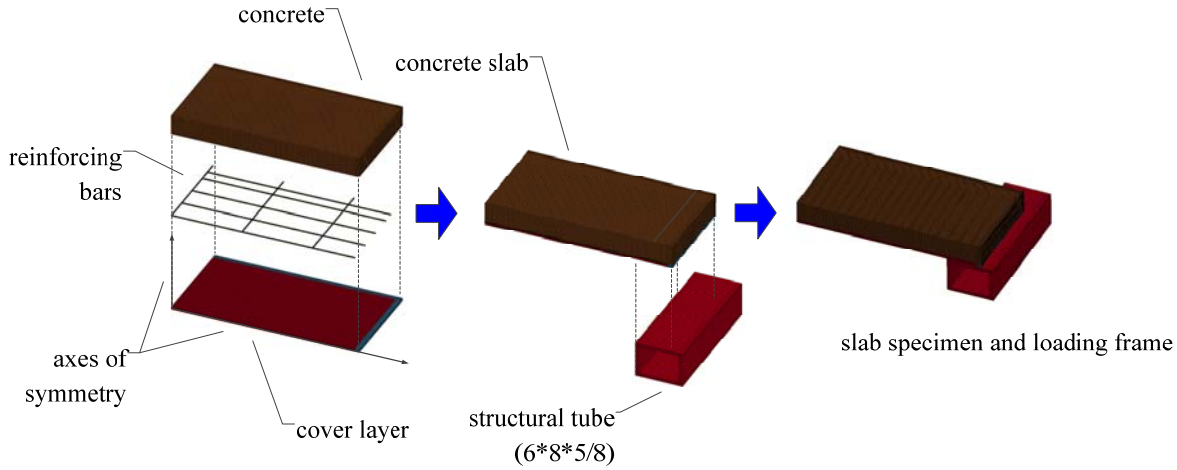

Figure 2. Layout of the ¼ FE model for the slab and the end support beam

As in the experiment, the slab is placed at both ends against two support steel box beams, which are included in the model domain but are essentially fully restrained on all sides except the top and inner surfaces. Considering the way the RC slab was placed against the supporting beams in the experiment, in which sliding was not restrained, a surface to surface contact is employed to model the interface between the RC slab and supporting steel beams, herein using the keyword *CONTACT_AUTOMATIC_SURFACE_TO_SURFACE [1] in LS-DYNA. No penetration is considered and the contact surface can transfer normal force but no shear or friction incurs. It is worth noting that the global slab response is found to be rather sensitive to whether or not sliding is allowed in the model.

2.3 Material models

2.3.1 Concrete

The concrete in the RC slab is modelled by KCC and CSC model respectively. For both models, automatic generation of parameters is employed by specifying an unconfined compressive strength. The compressive strength of the concrete is assumed to be 30MPa based on the experimental data.

The CSC model offers a unique feature which allows for the recovery of tensile damage when the stress reverts from a tensile to a compressive condition, thus enabling to a certain degree an anisotropic behaviour. In this simulation, the standard KCC model and two versions of CSC model (with/without anisotropy) are used at first and it is found that no major difference exists between using the two versions of CSC model. This suggests that the anisotropic property is not a significant factor in the present simulation. Thus, most of the analyses are carried out between the standard KCC and the CSC model without the tension-recovering feature, making the results more directly comparable.

Both models incorporate a length factor which relates to the characteristic mesh (element) size in the softening phase of the material response, such that the total fracture energy on a per-element basis will be equal to the specified fracture energy regardless of the mesh size. As a result, the stress-strain curve is rendered dependent upon the element size.

To evaluate the actual behaviour of the two models, numerical tests are conducted to demonstrate the stress-strain relationships resulting from the material model under various stress conditions. The numerical tests are carried out using a single element test approach. A single cubic element with a length of 6.35mm (identical to typical elements used in the slab model) is employed**Error! Reference source not found.**. In order to produce the whole stress-strain curve including the softening branch, the primary load is applied in a displacement-controlled manner by applying nodal velocities on the loading nodes in accordance with the intended loading pattern. Necessary constraints are also included to avoid unwanted rigid body motion.

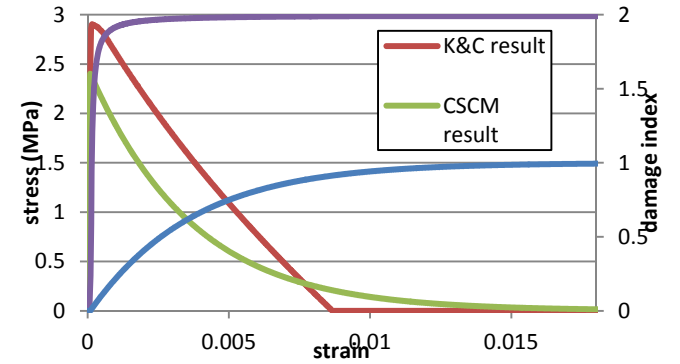

a) Uniaxial tension

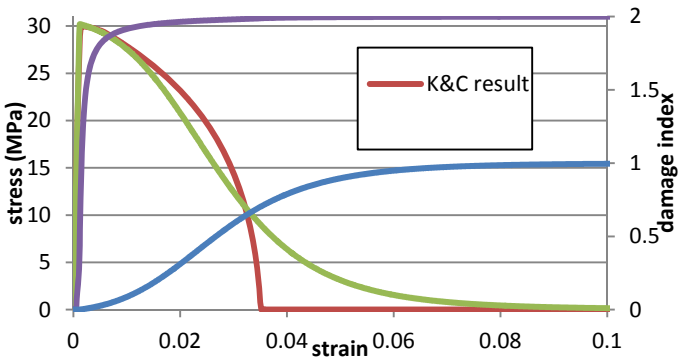

b) Uniaxial compression

Figure 3. Stress-strain curves produced by the two material models (element size = 6.35mm)

The comparison shows that the tensile strength achieved by the KCC model is slightly larger than the CSC strength, while the elastic modulus is identical. In the softening regime, the two curves tend to produce about the same integrated area under each curve, indicating that a similar amount of fracture energy is achieved in both models.

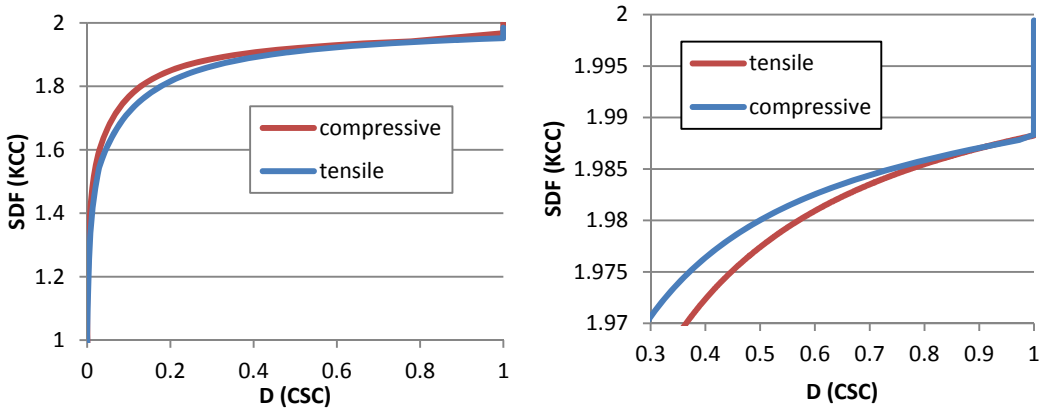

Figure 4. Relationship between SDF in KCC and D in CSC model

Different damage index are defined within the two material models, namely SDF in KCC and D in CSC model, to measure the damage accumulation. SDF is defined as follow:

$$SDF = \frac{2\lambda}{\lambda + \lambda_m} \tag{1}$$

where λ_m denotes the value λ at the maximum failure surface. As λ is a positive non-decreasing variable, SDF varies from 0 to 2. When λ equals λ_m, SDF=1, thus in the pre-peak phase 0<SDF<1. When concrete enters softening phase, 1<SDF<2. SDF approaches 2 when λ increases to infinity, which ultimately represents a total damage state.

The *D* index in CSC is a function of the current damage threshold τ, as:

$$\begin{cases} d^b = d(\tau^b) \\ d^d = d(\tau^d) \end{cases} \tag{2}$$

So two damage indexes, namely brittle and ductile damage d^b and d^d, respectively, are recorded separately by brittle and ductile damage threshold τ^b and τ^d. The brittle damage accumulation depends on the maximum principal strain and the ductile damage accumulation depends on the total strain components, with τ^b and τ^d defined respectively as follows:

$$\tau_b = \sqrt{E\varepsilon_{\max}^2} \tag{3a}$$

$$\tau_d = \sqrt{\frac{1}{2}\sigma_{ij}\varepsilon_{ij}} \tag{3b}$$

The damage index *D* is the current maximum between the brittle and ductile damage index, i.e, $D = \max(d^b, d^d)$.

As can be seen from Fig. 4, the D index appears to closely relate to the (descending) stress state and the absolute strain, which are both physically meaningful and are in line with what one would expect as damage accumulates. On the other hand, however, the way SDF is defined makes it less indicative of the continuous growth of damage and much of the descending branch falls into a narrow margin close to the maximum value of 2. Consequently, the identification of the material state towards severe damage and total failure becomes somewhat problematic using the SDF values.

Further discussion about the general inadequacy of such a damage indicator will be given elsewhere. For the purpose of assisting the interpretation of the damage development in the

later RC slab analysis, Fig. 4 also plots the relationship between SDF and the D index while SDF varies in a range of 1.97~2.0.

2.3.2 Steel rebar

The steel rebar is modelled using beam elements, for which the material model MAT_RC_BEAM [1] is adopted. This model takes into account the Bauschinger's effect by following a Ramberg-Osgood stress-strain relationship, as depicted in Fig. 5. Several key parameters of steel material used are listed in Table 1.

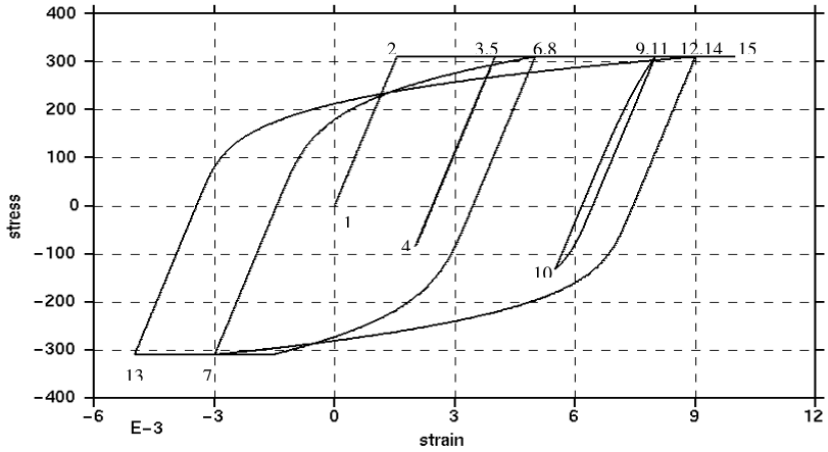

Figure 5. Stress-strain curve in the steel reinforcement model

Table 1: Key parameters used in the steel model

Young's modulus	Yielding stress	Ultimate stress	Strain begins to harden	Strain reaches ultimate stress
200GPa	60ksi (414MPa)	115ksi (792MPa)	0.00286	0.04

3. Simulation results of RC slab response to blast load and associated analysis

The numerical simulation results of the blast response of the RC slab using the two concrete models, respectively, are presented and discussed in this section. As mentioned in Introduction, the overall structural response is primarily monotonic and similar response characterises are expected to occur in general RC members involving rebar-concrete interaction mechanisms, barring abnormal material model behaviour.

3.1 Overall response and failure modes

The blast load is simulated by applying a uniformly distributed pressure onto the loading face of the RC slab. Fig. 6 shows the blast pressure time history considered in the present study.

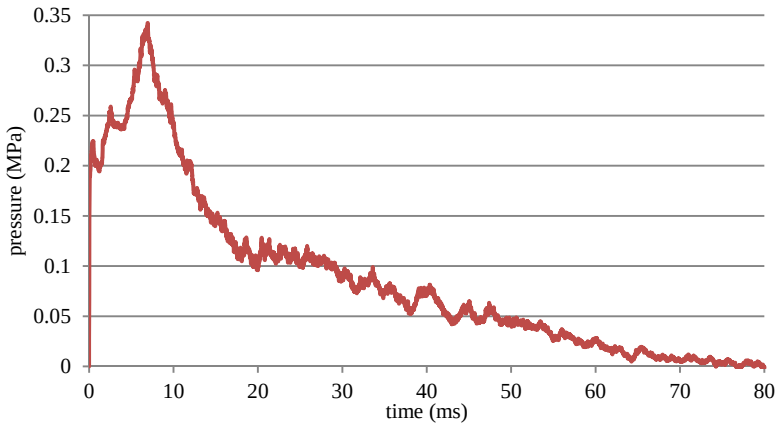

Figure 6. Time history of applied blast pressure (adapted from [10])

Fig. 7 shows the time histories of the central deflections in the models using KCC and CSC model, respectively. The results from both versions of the CSC models exhibit an increasing phase of the response to a limited peak deflection (about 90mm or 6.8 % of the net slab span), followed by a stable oscillation around a permanent plastic deformation. Both the pattern and magnitude of the response are consistent with the experimental observation. Since the results from both CSC models do not differ significantly, in the subsequent presentation only the results from the CSC-unrecoverable model are presented and compared with those from the KCC model.

The deflection time history from the KCC model shows almost identical initial increase phase of the response. However, the response does not stabilise as in the case of CSC model, and the deflection increases at somewhat a constant rate (i.e. constant velocity) after the initial phase of the response. This indicates that the RC slab becomes essentially a free flying object, which would only happen when a total global failure has taken place, and yet this was not the case from the experiment. It is noteworthy that the slab appears to have failed globally in the KCC model at about 13ms when a central deflection reaches only about 60 mm (or 4.5% of the net span), which is well below the peak deflection experienced in the CSC model. This observation is significant in that, irrespective of the comparison to the experimental result, the RC slab model based on KCC fails prematurely as compared to the CSC model.

The global failure of the RC slab model with KCC can also be observed from the time histories of the reaction forces against the applied blast load, as shown in Fig. 8. Both models achieved about the same magnitude of resistance capacity. However, the reaction force with KCC model drops sharply at about 13 ms, whereas that in CSC model it follows closely the path of the deflection into an oscillation phase.

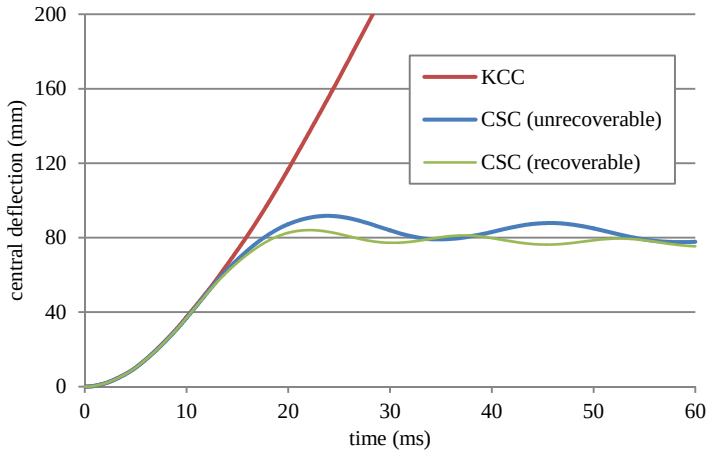

Figure 7. Time history of central deflection

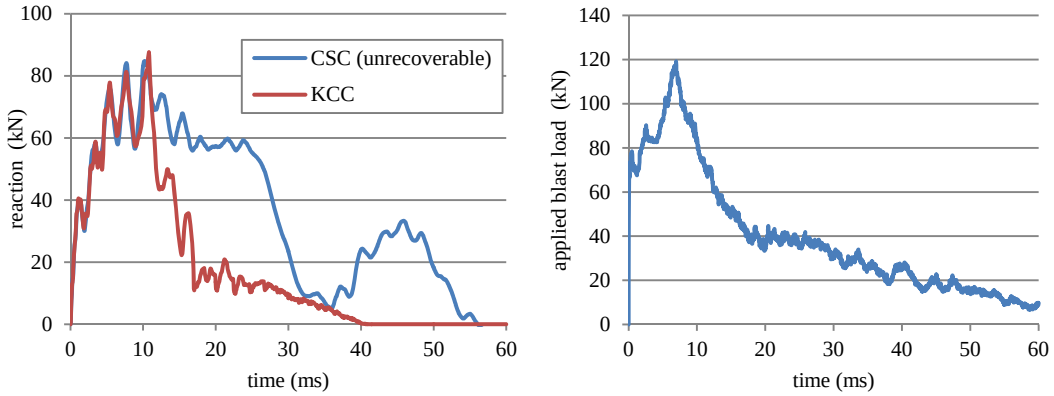

a) Reaction force b) Applied blast load

Figure 8. Time histories of reaction force and applied blast load (based on the ¼ model)

Fig. 9 compares the development of damage patterns (viewing from the tension side of the slab) between the KCC and CSC model at representative time steps. Note that in order to make the damage comparable, the scale of the SDF in KCC model is narrowed to a range of 1.97~2.0 against a range of 0.35~1.0 in CSC model in accordance with the calibration results shown earlier in Section 2.3.1.

It can be observed that the initial damage develops in a similar pattern between the two models. However, upon reaching the peak resistance at around 10 ms, the model with KCC concrete exhibits a rapid spread of damage in concrete stemming from the initial major

cracks and along the longitudinal reinforcing bars. In contrast, the damage in the model with CSC tends to stabilise with a final crack pattern featured by distributed lateral cracks together with longitudinal cracks along the main reinforcing bars, which agree favourably with the experimental observations.

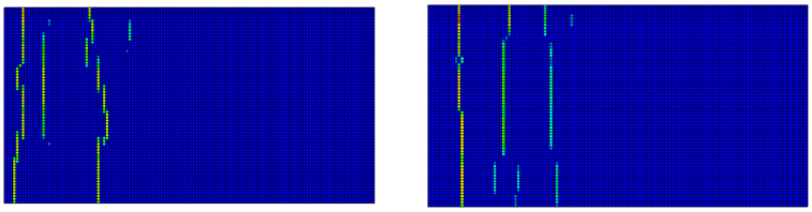

t=2ms (left: KCC_1.97~2.0; right: unrecoverable CSC_0.35~1.0)

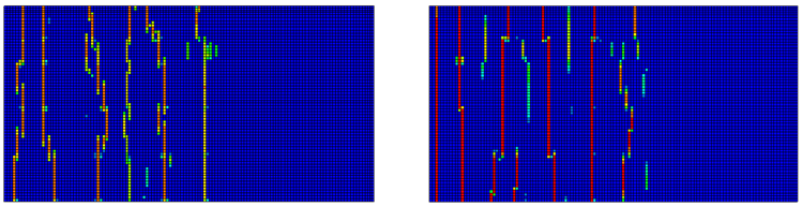

t=4ms (left: KCC_1.97~2.0; right: unrecoverable CSC_0.35~1.0)

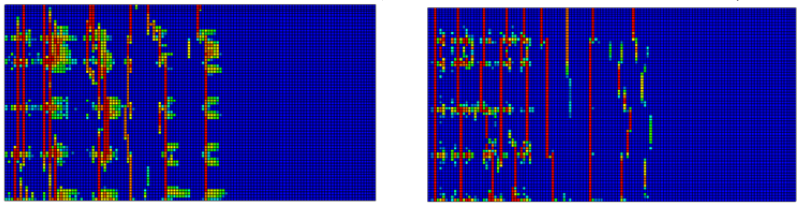

t=8ms (left: KCC_1.97~2.0; right: unrecoverable CSC_0.35~1.0)

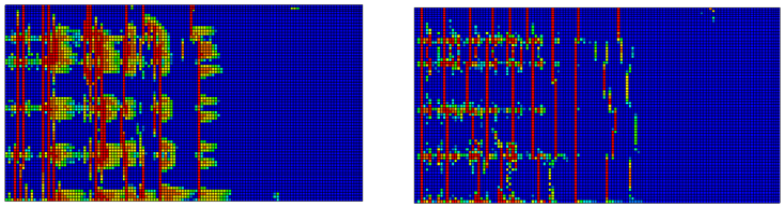

t=10ms (left: KCC_1.97~2.0; right: unrecoverable CSC_0.35~1.0)

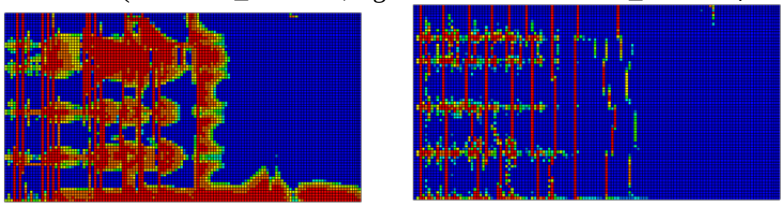

t=12ms (left: KCC_1.97~2.0; right: unrecoverable CSC_0.35~1.0)

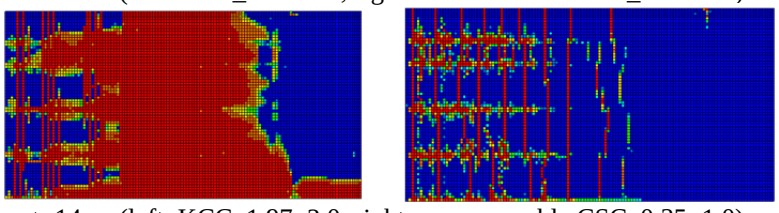

t=14ms (left: KCC_1.97~2.0; right: unrecoverable CSC_0.35~1.0)

Figure 9. Damage as viewing from the slab surface opposite to the blast load

3.2 Damage distribution over the slab depth

To assist in the diagnosis of the cause of the distinctive behaviour of the two slab models, the development of damage is further examined from a longitudinal cross-sectional point of view. One cross sectional cut is taken at the position of a longitudinal bar and another in-between two adjacent bars. The developments of the damage patterns at these two longitudinal cross-sections are presented in Fig. 10 and 11, respectively.

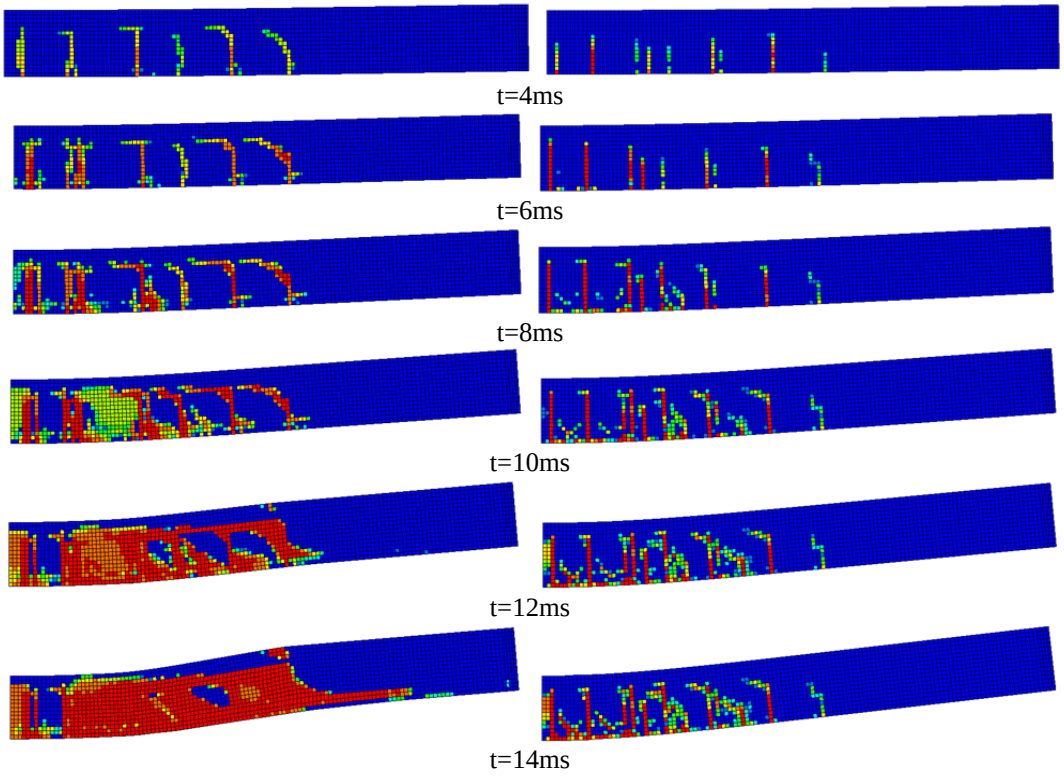

Figure 10. Damage patterns at rebar position (left: KCC_1.97~2.0; right: CSC_0.35~1.0)

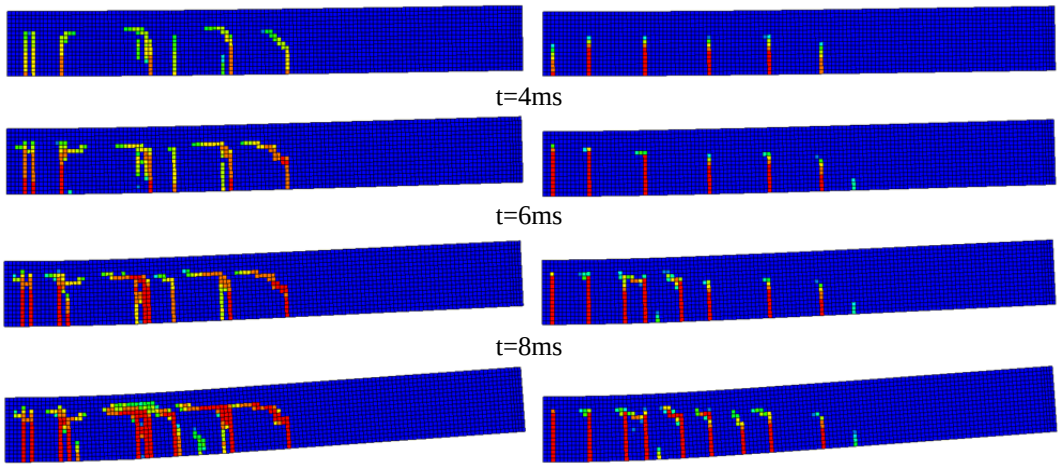

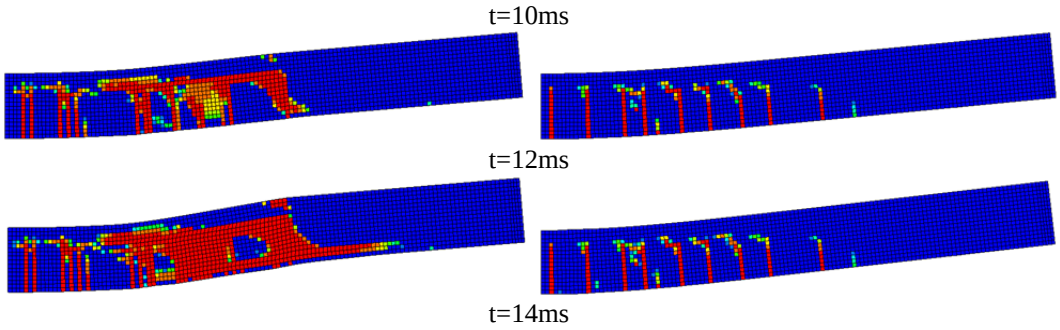

Figure 11 Damage patterns at position in between rebars (left: KCC_1.97~2.0; right: CSC_0.35~1.0)

The damage patterns at the two cross sections in the same model are generally consistent with each other, so the following discussion will be based on the damage patterns as observed at the cross section along the longitudinal bar shown in Fig. 10.

In both KCC and CSC models, damage initiates as bending cracks, starting from the mid-span region and then propagating towards the support as can be expected in a global mode governed response. The overall crack patterns appear to be generally comparable between the two models until around the time when the maximum resistance is reached (10 ms). After that, wide-spread failure in concrete through the slab depth occurs in the KCC model, whereas the CSC model reaches a stabilised crack pattern typical of a reinforced concrete member under bending.

The spread of failure in concrete in the KCC model appears to eventually result in the longitudinal rebar being pulled through over the anchorage region up to the position of the support at about 14 ms, and this is believed as the main trigger of a complete loss of the global resistance of the slab.

A closer inspection of the crack patterns in Fig. 10 reveals that inclined cracks actually appear early in the KCC model, and these cracks extend from the top of the bending cracks towards the position of the neutral axis, promoting the development of horizontal cracks along the neutral axis level where higher shear stress occurs. The horizontal cracks continue to develop and eventually coalesce to from a continuous longitudinal crack line, which appears to break the slab section. The slab would have lost much of its global resistance due to the above shear effect even if the rebar did not lose interaction with the surrounding concrete.

The development of premature shear failure of concrete in the RC slab with the KCC concrete model can be directly observed from the shear stress and shear strain contours over the longitudinal cross section, as shown in Fig. 12 and 13, respectively. While the slab with CSC model maintains an effective shear force transfer mechanism throughout the main response period, the shear stress transfer diminishes in the slab with KCC model in the post-peak resistance phase, and at the same time considerable shear deformation develops over the high shear zones, particularly along the neutral axis and the longitudinal rebar positions, resulting in two apparent horizontal tearing failure lines.

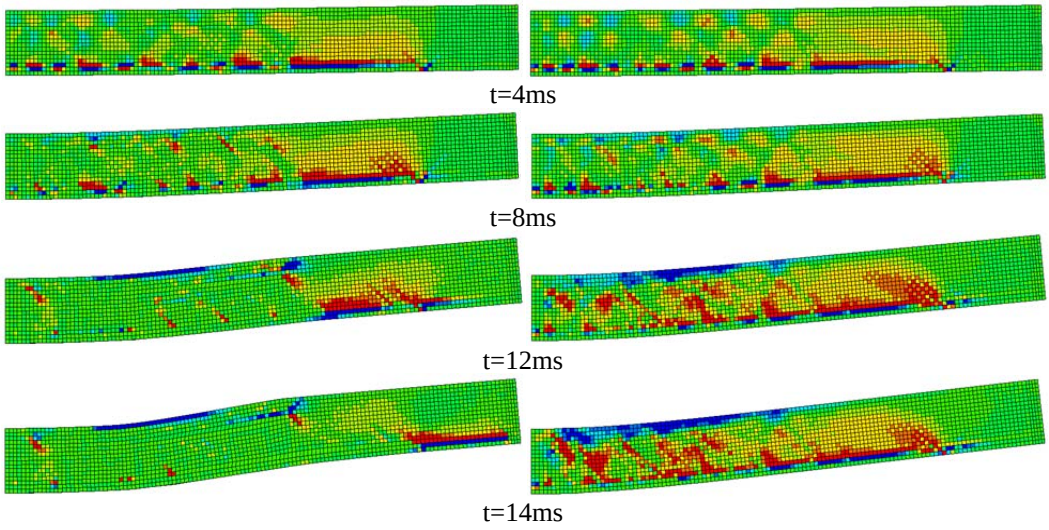

Figure 12. Shear stress distributions over the longitudinal cross section through a rebar position (left: KCC; right: CSC; range: -3.0 ~ +3.0 MPa)

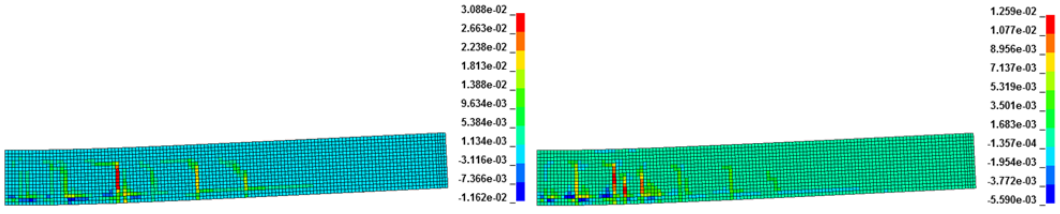

t=8ms (left KCC: -0.012~0.031; right CSC: -0.006~0.013)

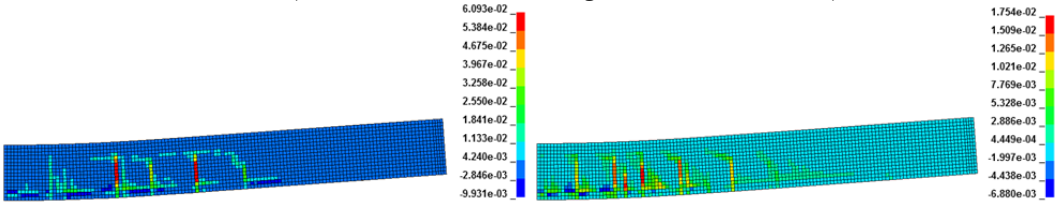

t=10ms (left KCC: -0.001~0.061; right CSC: -0.007~0.018)

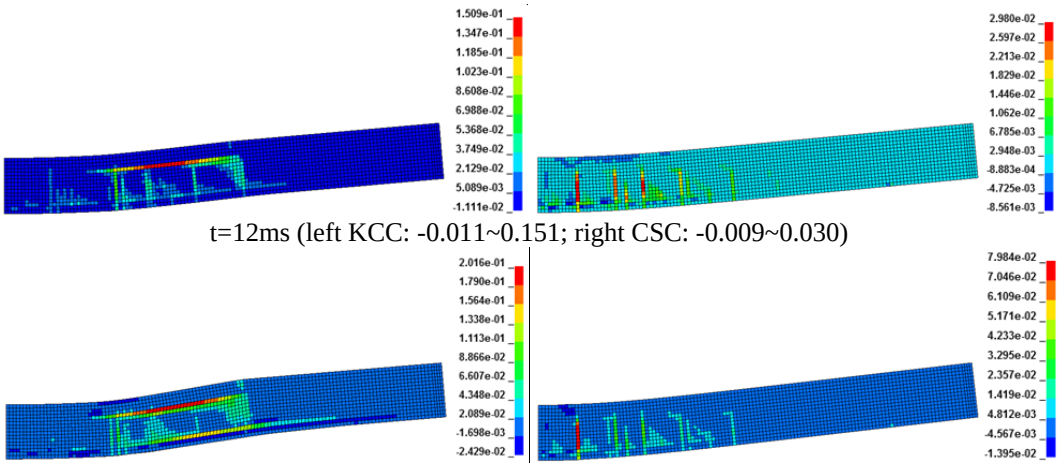

Figure 13. Shear strain distributions over the longitudinal cross section through a rebar position (left: KCC; right: CSC)

3.3 Evolution of stress/damage in rebar and surrounding concrete

Fig. 14 presents the evolution of the axial stress distribution in rebar at selected time instants. At the early stage of the response up to about 8 ms, the axial stress in the rebar develops in a similar fashion in both KCC and CSC models, and is consistent with a flexure-controlled response under a distributed load. The “bond” stress in the surrounding concrete, which is correlated to the slope of the axial stress in the rebar, generally increases from the mid-span outward and becomes larger in the “anchorage” zone near the end support (note that the inner edge of the support area is at about 650mm from the mid-span). Note also that the local fluctuation of the axial stress in the rebar reflects the local variation of the “bond” stress in-between flexural cracks, as can be expected.

When the global response reaches a certain limit, herein at about 10ms, the stress in the rebar stops increasing in the KCC model, indicating that the “bond” stress in the surrounding concrete has reached its limit shear capacity. As the deformation further increases, the slope of the rebar stress in the mid-span region becomes flattened (at about 12-13ms) due apparently to the loss of (bond) strength in the surrounding concrete. This pushes up the (bond) stress in the anchorage region, leading to a progressive failure of the anchorage zone and eventually the global collapse of slab.

Comparing to the KCC model, the axial stress in the CSC model exhibits a consistent but globally increasing pattern as the response develops to reach the peak deformation. There is no sign of significant (bond) failure in the surrounding concrete.

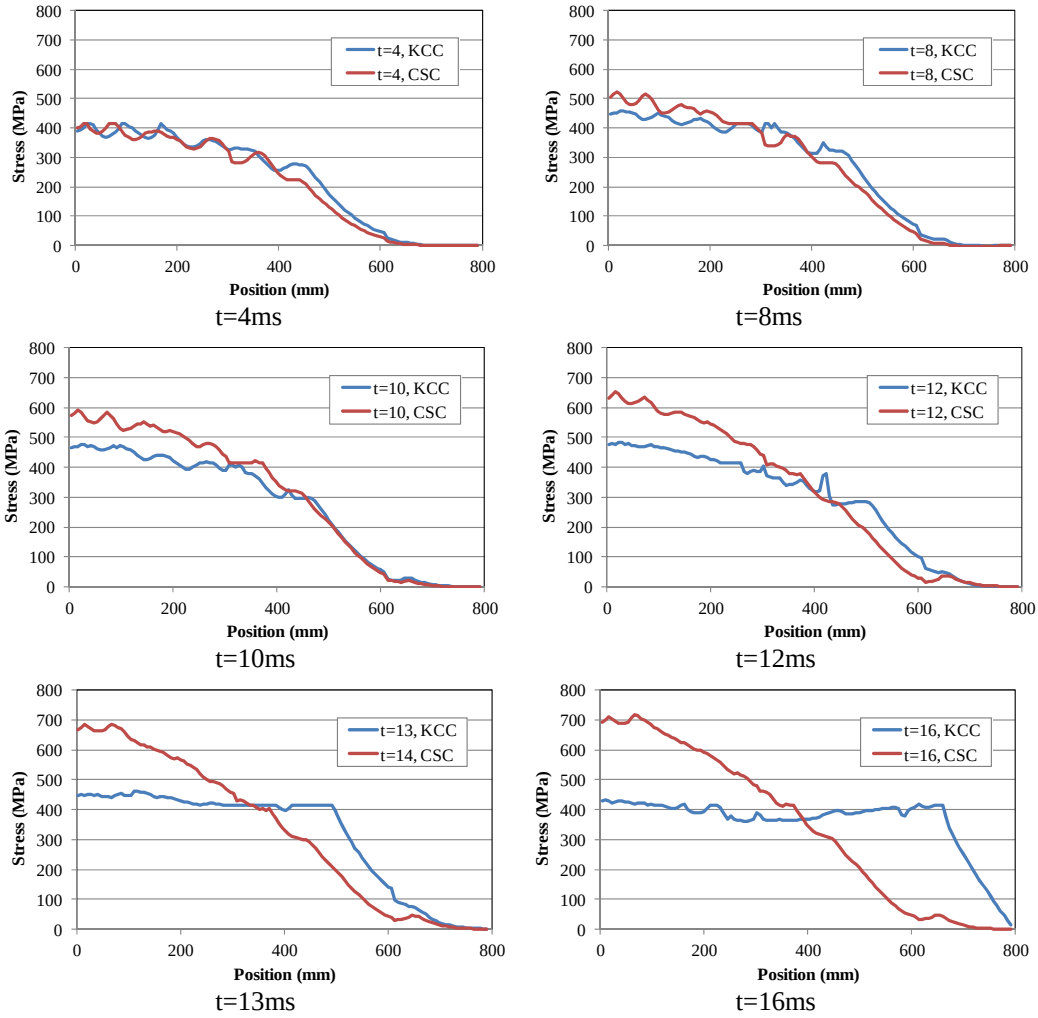

Figure 14. Development of axial stress distribution along longitudinal rebar (t: ms)

4. Discussion on the cause of abnormal simulation results with the KCC model

To further examine the process of the KCC concrete failure in shear (or "bond") around the longitudinal rebar, a column of concrete elements immediately surrounding a longitudinal rebar is taken out from the slab**Error! Reference source not found.** to expose the path to failure in the interaction between steel rebar and adjacent concrete.

A check of the responses among the four concrete elements at the same cross-section has found that the two elements on the left and right of the rebar generally have a similar

stress/strain level, so the mean values are taken between these two elements. On the other hand, elements above and below the rebar show slightly more different stress/strain states.

Figure 15 shows the development and distribution of damage in these concrete elements along the length of the rebar, for the KCC and CSC models, respectively. The general development paths confirm the observations made in Section 3.3 based on the rebar stress, in that a total (shear) failure eventually develops in the concrete elements along the rebar length in the KCC model, resulting in the loss of rebar effect on the concrete slab response and the global failure of the slab. Such a problem does not occur in the CSC model.

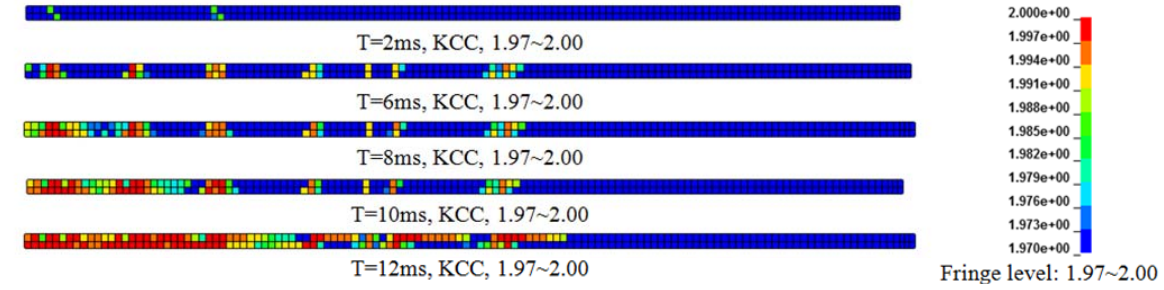

a) KCC model

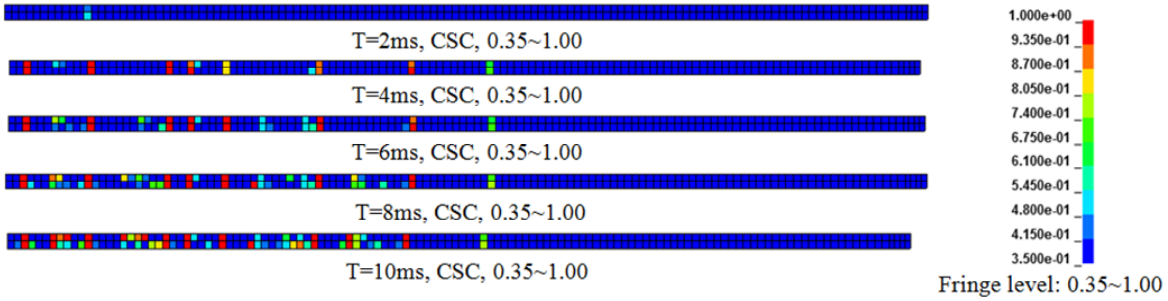

b) CSC model

Figure 15. Development and distribution of damage in concrete elements connected with rebar

In an attempt to explain what aspects in the KCC model have contributed in the abnormal simulation phenomenon, the shear and principal tensile strains in the concrete element connected to the rebar are extracted for different response levels. The results for the principal tensile strain are shown in Fog. 16. The limiting tensile strain at which the KCC model would completely lose its strength (thus becomes stress-less) for the size of the elements under a uniaxial tension condition is also shown on the plots for a benchmark purpose.

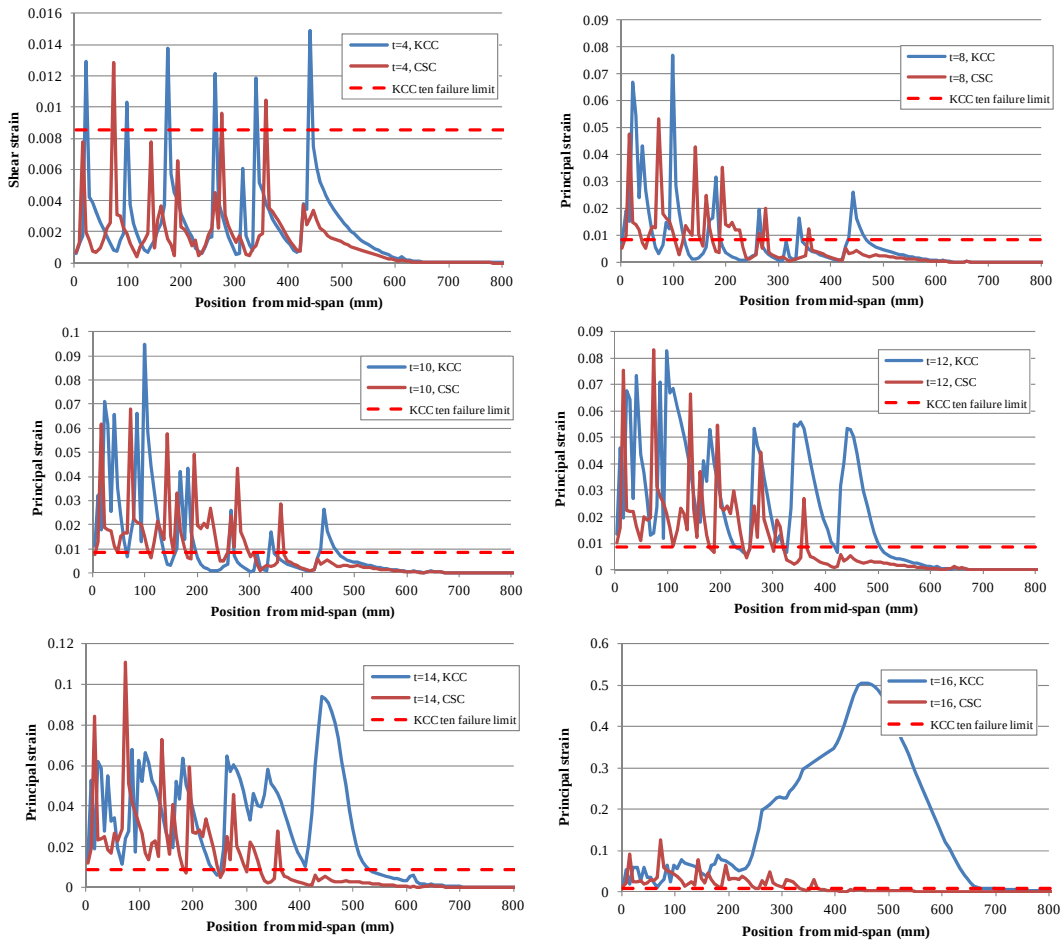

Figure 16. Principal (tensile) strain in concrete elements connected to rebar (t: ms)

From the shear/principal strain development, it can be observed that in the early stage of the response up to about 8ms, both the magnitudes and distributions of the strains do not differ significantly between the two models. However, with further increase of the shear/principal strains, the magnitude of the strains at the peak locations reach and exceed the KCC total failure limit, rendering the respective concrete elements to be totally stress-less. This in turn accelerates the increase of the strains in the concrete elements in general as the global response increases, and at the same time the peak strain bands widen much more quickly as compared to the CSC model. Finally, almost the entire set of the concrete elements connected to the rebar exceeds the total failure strain limit and thus enters into a stress-less state, leading to the collapse of the slab.

Based on the above results in conjunction with the comprehensive observations of the failure processes in the two models presented in the previous section, it may be concluded that the deterioration rate of tensile/shear strength in the softening stage in the KCC model,

particularly the progress into a zero stress state, tends to be too quick and too early. This feature may not pose any significant problem in high pressure applications, but could be problematic in lower pressure applications where tension and shear failure generally plays a governing role. The problem will tend to get worsened in reinforced concrete members such as the RC slab in the present investigation, where premature failure of concrete in shear and “bond” will result in an unrealistic elimination of the reinforcement effect, leading to a premature collapse of the RC member as if it was un-reinforced in the late stage of the response.

The isotropic damage feature of the material model, which manifests as an inability of recovering a reasonable compressive strength following the accumulation of tensile damage, would also contribute towards an accelerated deterioration of the integrity in a reinforced concrete member model. For instance, a concrete element which is failed by bending stress will be unable to transfer any other state of stress, even compression, which could be developed in the subsequent course of the response. Nevertheless, this aspect of shortcomings in the material model is not deemed to have played a significant role in the current RC slab example, as the same problem exists in the “unrecoverable” version of the CSC model which is adopted in the present investigation but no apparent global response anomaly has occurred therein.

The rectification of the problem with too quick a descending rate into a zero-stress state could be made with an appropriate modification of the residual strength surface. In its current setting, KCC model adopts a residual strength surface which starts from the origin and no residual shear strength can be developed in the negative pressure region, whereas in CSC model the stress deterioration is realised by applying scaled factor onto the original shear strength surface, which leads to a non-zero residual shear strength in the triaxial extension region. Another possible way of correcting the rapid attainment of a zero-stress state may be to implement a more gradual increase of the damage accumulation in the late stage of the softening phase.

5. Concluding remarks

A comparative numerical simulation study has been conducted in which two representative concrete material models, namely KCC and CSC models, are employed to model a typical RC slab subjected to blast load. The problem is generally in a global flexure regime and the response is primarily of a monotonic character. For such a classical modelling situation,

however, the two models exhibit very distinctive performances. In particular, the model with KCC concrete material tends to fail prematurely with a total global failure of the slab, which is not consistent either with the experimental observations or with the CSC modelling results.

An extensive analysis of the failure processes in the simulated results reveal that the global failure in the slab with the KCC model is caused by two premature shear failure lines, one horizontally at the neutral axis level in the high shear region, and another along the longitudinal rebar position. The former leads to an effective break-up of the slab along the shear failure line, while the latter eventually results in the reinforcing bars being pulled through in the concrete, which effectively eliminates the reinforcement effect and causes the collapse of the slab.

The aspects of the KCC material model behaviour that may be linked to the abnormal performance of the RC slab simulation are deemed to include, primarily, the rapid descending rate in the later softening phase and an earlier entry into a stress-less state. While this feature may not pose a significant problem in high pressure applications, it becomes problematic in low pressure situations, especially in a reinforced concrete structure such as in the RC slab under investigation where premature failure of concrete in shear and “bond” will accelerate unrealistically the failure process towards a premature collapse.

The rectification of the problem with too quick a descending rate into a zero-stress state could be made with an appropriate modification of the residual strength surface. Another possible way of correcting the rapid attainment of a zero-stress state may be to implement a more gradual increase of the damage accumulation in the late stage of the softening phase. A more detailed investigation into these modification options will be reported in a subsequent study.

References

[1] LSTC, LS-DYNA Keyword User’s Manual Volume I, 2012.

[2] ANSYS, AUTODYN ® User Manual Version 12.0, Canonsburg, US, 2009.

[3] ABAQUS Analysis User’s manual. Version 6.7, Karlsson & Sorensen, Inc., 2007.

[4] Tu, Z., Lu, Y., Evaluation of typical concrete material models used in hydrocodes for high dynamic response simulations, *International Journal of Impact Engineering*, 2009, 36, 132–146.

[5] Malvar, L., Crawford, J., A plasticity concrete material model for DYNA3D, *International Journal of Impact Engineering*, 1997, 19, 847–873.

[6] Murray, Y.D., Users Manual for LS-DYNA Concrete Material Model 159, 2007.

[7] ARUP, Verification of the Karagozian and Case Material-Model for LS-DYNA 971 R3, Report, 2009.

[8] Wu, Y., Crawford, J., Magallanes, J., Performance of LS-DYNA® Concrete Constitutive Models, in: 12th International LS-DYNA Users Conference, Dearborn, Michigan USA, 2012, 1-14.

[9] Tu, Z., Lu, Y., Modifications of RHT material model for improved numerical simulation of dynamic response of concrete, *International Journal of Impact Engineering*, 2010, 37, 1072–1082.

[10] University of Missouri-Kansas City, Blast Blind Simulation Contest, Http://sce.umkc.edu/blast-prediction-contest/, retrieved June 2013.